How Marine Emissions of Bromoform Impact the Remote Atmosphere

Yue Jia[1], Susann Tegtmeier[1], Elliot Atlas[2], Birgit Quack[1]

[1]GEOMAR Helmholtz Centre for Ocean Research Kiel, Kiel, Germany

[2]University of Miami, 4600 Rickenbacker Causeway, Miami, USA

correspondence to: Yue Jia (yjia@geomar.de)

Atmospheric
Chemistry
and Physics
Discussions

Open Access

10   **Abstract**

11   Oceanic emissions of very short lived halocarbons (VSLH), such as $CHBr_3$, are important for the halogen

12   budget of the atmosphere. It is an open question how localized elevated emissions in coastal and

13   upwelling regions and low background emissions, typically found over the open ocean, impact the

14   atmospheric VSLH distribution. In this study, we use the Lagrangian dispersion model FLEXPART to

15   simulate atmospheric $CHBr_3$ resulting from uniform background emissions, on the one hand, and from

16   elevated emissions observed during three tropical cruise campaigns, on the other hand.

17   The simulations demonstrate that the atmospheric $CHBr_3$ distributions due to uniform background

18   emissions are highly variable with accumulations taking place in regions of low wind speed. This relation

19   holds on regional and global scales demonstrating the importance of the atmospheric transport for the

20   distribution of short-lived trace gases with lifetimes in the range of days to weeks.

21   The impact of localized elevated emissions, measured during three research cruises, on the atmospheric

22    $CHBr_3$ distribution varies significantly from campaign to campaign. The estimated impact depends on

23   the strength of the emissions and the meteorological conditions. In the open waters of the western Pacific

24   and Indian Ocean, localized elevated emissions only slightly increases the background concentrations of

25   atmospheric $CHBr_3$, even when 1° wide source regions along the cruise tracks are assumed. Near the

26   coast, elevated emissions, including hotspots up to 100 times larger than the uniform background

27   emissions, can be strong enough to be distinguished from the atmospheric background. However, it is

28   not necessarily the highest hotspot emission that produces the largest enhancement, since the tug-of-war

29   between fast advective transport and local accumulation at the time of emission is also important.

30   Our analyses contribute to a better understanding and prediction of the timing and regional characteristics

31   of tropospheric $CHBr_3$ distribution. Significantly, our results demonstrate that transport variations of the

32   atmosphere itself are sufficient to produce highly variable VSLH distributions, and elevated VSLH in

33   the atmosphere do not always reflect a strong localized source. Localized elevated emissions can be

34   obliterated by the highly variable atmospheric background, even if they are orders of magnitude larger

35   than the average open ocean emissions.

36

37   **1. Introduction**

38

39   Very short lived halocarbons (VSLHs) with atmospheric lifetimes shorter than 6 months have natural

40   oceanic sources which are dominated by brominated and iodinated compounds (Carpenter and Liss, 2000;

41   Quack et al., 2004; Law et al., 2006). VSLHs have drawn considerable interest due to their contribution

42   to stratospheric ozone depletion and tropospheric chemistry (Solomon et al., 1994; Dvortsov et al., 1999;

43   Salawitch et al., 2005; Feng et al., 2007; Tegtmeier et al., 2015; Hossaini et al., 2015). In this work, we

44   focus on the VSLH bromoform ($CHBr_3$), since most organic oceanic bromine is released into the

45   atmosphere in this form.

46      $CHBr_3$ concentrations measured in ocean waters are characterized by large spatial variability with

47   elevated abundances in phytoplankton blooms (Baker et al., 2000, Liu et al., 2013) and equatorial and

48   upwelling regions due to biological sources (Carpenter et al., 2009; Quack and Wallace, 2003; Quack et

49   al., 2007; Fuhlbrügge et al., 2016). The open ocean generally shows quite homogeneous, low $CHBr_3$

50   concentrations, compared to higher concentrations and strong gradients found in coastal and shelf areas

51   (Quack and Wallace, 2003), At the coast, high oceanic concentrations are related to macro algae (Klick

52   and Abrahamsson, 1992) and anthropogenic sources (Boudjellaba et al., 2016) such as power plants

53   (Yang, 2001) and desalination facilities (Agus et al., 2009).

54   Due to sparse measurements and limited process understanding, existing estimates of global air-sea flux

55   distributions of $CHBr_3$ and other VSLHs are subject to large uncertainties (e.g. Warwick et al., 2006;

56   Palmer and Reason, 2009; Liang et al., 2010; Ordóñez et al., 2012; Stemmler et al., 2013; Ziska et al.,

57   2013; Carpenter et al., 2014). Open ocean background emissions of $CHBr_3$ are modeled to be around

58   100 pmol m^{-2} hr^{-1} (Ziska et al., 2013), consistent with simultaneous in-situ measurements of air and water

59   concentrations (Butler et al., 2007; Liu et al., 2013; Fiehn et al., 2017). The spatial and temporal

60   distribution of elevated emissions in coastal and upwelling regions is currently based on very limited

61   observations. Campaigns in these regions suggest that emissions generally increase near coastlines, and

62   that sporadic peak emissions with extremely high values can be found (e.g. Butler et al., 2007; Liu et al.,

63   2013; Fuhlbrügge et al., 2016; Fiehn et al., 2017). Analysis of the measurements suggests that such peak

64   emissions are often of limited spatial extent and cover not more than a distance of 50-100 km along the

65   cruise track. We will use the term 'elevated emissions' when describing emissions that are on average

66   up to a factor of 10 larger than the background and 'hotspot emissions' for sporadic emissions up to a

67   factor of 100 larger than the background.

68   There are two main approaches to derive the magnitude of VSLH emissions, i.e. "bottom-up" approach

69   (e.g. Quack and Wallace, 2003; Carpenter and Liss, 2000; Butler et al., 2007; Ziska et al., 2013) and

70   "top-down" approach (e.g. Warwick et al., 2006; Liang et al., 2010; Ordóñez et al., 2012). For the

71   "bottom-up" method, measured surface sea water concentrations of VSLHs at the "bottom" (surface) are

72   extrapolated to estimate global emissions. For the "top-down" method, the emissions of VSLHs are

73   constrained by the measured abundances at the "top" (atmosphere) so that model simulations based on

Atmospheric
Chemistry
and Physics
Discussions

74   the constrained global emission estimates reproduce the observed atmospheric concentrations. These two

75   approaches yield different estimates of the global VSLHs emissions, with the recent "top-down"

76   approaches resulting in generally higher emissions than the recent "bottom-up" approaches.

77   In the tropical ocean waters of the Atlantic, the western Pacific and Indian Ocean, the existence of

78   localized elevated $CHBr_3$ emissions and hotspots has been confirmed (Butler, et al, 2007; Liu et al., 2013;

79   Krüger and Quack, 2013; Quack and Krüger, 2013; Fiehn et al., 2017). At the same time, these

80   convectively active regions offer an efficient pathway for the vertical transport of short-lived oceanic

81   compounds from the boundary layer to the stratosphere (e.g. Aschmann et al., 2009; Hossaini et al., 2012;

82   Tegtmeier et al., 2012, 2013; Marandino et al., 2013; Liang et al., 2014). Moreover, the Asian monsoon

83   has been recognized as an efficient transport pathway for short-lived pollutants and VSLHs (Randel et

84   al., 2010; Hossaini et al., 2016; Fiehn et al., 2017). Given that elevated oceanic $CHBr_3$ emissions are

85   expected to occur in the same regions as strong convection, it is of interest to analyze how these elevated

86   emissions impact $CHBr_3$ in the atmospheric boundary layer, which feeds into the upward transport.

87   Measurements of $CHBr_3$ abundance in the atmospheric boundary layer show large spatial variability (e.g.,

88   Quack and Wallace, 2003; Montzka and Reimann, 2011; Lennartz et al., 2017). A compilation of

89   available measurements by Ziska et al. (2013) suggests similar $CHBr_3$ distribution patterns in the

90   atmospheric boundary layer as in the surface ocean, with higher mixing ratios in the equatorial, coastal

91   and upwelling regions. However, given the sparse data base and the uncertainties in the spatial and

92   temporal extent of oceanic emissions, the detailed distribution of boundary layer $CHBr_3$, cannot be well

93   constrained (e.g., Hepach et al., 2014; Fuhlbrügge, et al., 2013). On the one hand, the spatial and temporal

94   extent of elevated localized emissions is usually unknown, leading to large uncertainties when estimating

95   their overall magnitudes. On the other hand, the influence of meteorological conditions, distinctive

96   transport patterns and variations of atmospheric sinks, such as the background OH field (e.g. Rex et al.,

97   2014), can be expected to modulate the effect of elevated oceanic sources. Therefore, it is still an open

98   question of the magnitude of elevated and hotspot emissions on the local atmospheric $CHBr_3$ distribution.

99   Such knowledge is relevant to understand the importance of localized elevated emissions for atmospheric

100   abundances and to interpret existing atmospheric measurements with respect to potential sources and

101   driving factors.

102   In this study, we use observational data from three tropical research cruises, one in the Indian Ocean

103   (OASIS) and two in the western Pacific (TransBrom and SHIVA). We use the Lagrangian particle

104   dispersion model FLEXPART to investigate the transport and atmospheric distribution of VSLHs.

105   Taking bromoform ($CHBr_3$) as example, we compare the atmospheric signals estimated from the elevated

106   and hotspot emissions measured during the ship campaigns to the distribution derived from only uniform

107   background emissions. The campaigns and the FLEXPART model are introduced in Sect. 2. In Section

108   3, we discuss the distributions and variability of atmospheric $CHBr_3$ based on uniform background

109   emissions. We present the observed hotspots of $CHBr_3$ emissions in Section 4.1, and compare the

110   simulated atmospheric mixing ratios resulting from elevated emissions during three campaigns with the

111   background values (Section 4.2). Conclusions are given in Section 5.

112

113   **2. Data and Methods**

114

115   **2.1 Background and in-situ CHBr$_3$ emissions**

116

117   In this study, we distinguish between open ocean background and in-situ CHBr$_3$ emissions. Open ocean

118   emissions are deduced to be around 100 pmol h^{-1} m^{-2} based on global bottom up scenarios (Quack and

119   Wallace, 2003, Ziska et al., 2013). While emissions for individual regions and seasons can be higher or

120   lower than this, including negative fluxes going from the atmosphere into the ocean, 100 pmol h^{-1} m^{-2}

121   represents the typical mean value averaged over all oceanic basins between 60°S and 60°N. The

122   background open ocean emissions exclude by design emissions from coastal, shelf and upwelling regions.

123

124   In-situ oceanic emissions of CHBr$_3$ have been calculated from the observational data collected during

125   three tropical ship campaigns. The two campaigns TransBrom (October 11th-23rd, 2009, Krüger and

126   Quack, 2013) and SHIVA (November 15th-28th, 2011, Quack and Krüger, 2013) took place in the

127   western Pacific, while the OASIS campaign (July 11th-August 6th, 2014, Fiehn et al., 2017) was

128   conducted in the western Indian Ocean. During each campaign, surface air and water samples were

129   collected simultaneously at regular intervals (every 3 to 6 hours). The emissions were calculated from

130   these co-located data and the instantaneous wind speed (Ziska et al., 2013, Fuhlbrügge et al., 2016, Fiehn

131   et al., 2017). The detailed cruise track and the magnitude of the oceanic CHBr$_3$ emissions of each

132   campaign is given in Fig. 1. The in-situ emissions include both open-ocean emissions and elevated

133   emissions from coastal, shelf and upwelling regions with our evaluations focusing on the regions of

134   elevated emission.

135

136   **2.2 Modeling**

137

138   For the simulations of the atmospheric distribution and transport of CHBr$_3$, we used the Lagrangian

139   particle dispersion model, FLEXPART (Stohl et al., 2005), which has been validated by previous

140   comparisons with measurements (Stohl et al., 1998; Stohl and Trickl, 1999). Lagrangian particle models

141   such as FLEXPART compute trajectories of a large number of so-called particles, presenting

142   infinitesimally small air parcels, to describe the transport, diffusion and chemical decay of tracers in the

143   atmosphere. The model includes turbulence in the boundary layer and free troposphere (Stohl and

144   Thomson, 1999) and a moist convection scheme (Forster et al., 2007) following the parameterization by

145   Emanuel and Živković-Rothman (1999). The representation of convection in FLEXPART simulations

146   has been validated with tracer experiments and ^{222}Rn measurements (Forster et al., 2007). Chemical or

147   radioactive decay of the transported tracer is accounted for by reducing the particle mass according to a

148   prescribed lifetime of the tracer. Alternatively, the loss processes can be prescribed via OH reaction

149   based on a monthly averaged 3 dimensional OH-field. In this study, we employ FLEXPART version

150   10.0, which is driven by 3-hourly meteorological fields from ECMWF (European Centre for Medium-

151   Range Weather Forecasts) reanalysis product ERA-Interim (Dee et al., 2011) with a horizontal resolution

152   of 1º x 1º and 61 vertical model levels.

153   We performed two kinds of simulations based on the different emission scenarios. The first one used the

154   uniform global background emission, and the second one used in situ emissions observed during

155   individual ship campaigns. Chemical decay of $CHBr_3$ was simulated by prescribing a lifetime of 17 days

156   during all runs (Montzka and Reimann, 2011). For the background runs, a uniform air-sea flux of 100

157   pmol h^{-1} m^{-2} is prescribed over all ocean surface area between 60°S and 60°N. Three runs are conducted

158   covering the time period of the campaigns with a 1-month spin-up period in each case to reach a stable

159   background concentration in the atmosphere.

160   For the in-situ emissions of each campaign, simulations are based on the calculated $CHBr_3$ air-sea flux

161   (see Fig. 7, detailed description in Sec 4), which is released along the cruise track. The periods of these

162   campaign simulations are the same as the corresponding background simulations with emissions over

163   the whole time period. For each observational data point, an emission grid cell centered on the

164   measurement location is created. These grid cells are designed to be adjacent along the cruise track and,

165   based on the density of the measurements, are about 0.1 – 2.0° wide in cruise track direction. The grid

166   cells are chosen to be of a fixed width (0.5° or 1°) in the other direction and thus add up to the narrow

167   band of 0.5° or 1° width centered along the cruise track (Fig. 1). Our design of the emission grid cells

168   assumes that the elevated emissions can extend over a distance of 0.5°-1°. This choice has been motivated

169   by the spatial variability of the measurements along the cruise track (see also section 4.1 and Fig. 7).

170   Elevated emissions larger than 1000 pmol h^{-1} m^{-2} are found at 77 different locations along the three cruise

171   tracks examined in this paper. Out of the 77 measurements, only 11 correspond to singular locations with

172   no adjacent high emissions at the neighboring points. The other 66 measurements cluster together at 18

173   different locations with at least two adjacent observational points showing emissions larger than 1000

174   pmol h^{-1} m^{-2}. We define the length of such a location of elevated emissions as the distance between the

175   first and last data point with an air-sea flux exceeding 1000 pmol h^{-1} m^{-2}. Most of the 18 locations extent

176   over a distance larger than 0.5° (13 out of 18) and nearly half are larger than 1° (8 out of 18) supporting

177   our choice of the width of the emissions grid cells. Note that at the same time, the spatial extent of the

178   hotspots is comparable to the wind field resolution that drive our trajectory simulations. The amount of

179    $CHBr_3$ released from each grid cell is determined by the observational air-sea flux of the corresponding

180   data point and scales with the width of the narrow emission band described above. The specified $CHBr_3$

181   emission from each cell is kept constant for the duration of the model run and distributed over a fixed

182   number of trajectories. In order to capture the small scale processes (e.g. convection), the large number

183   of 2000, and 20000 trajectories are chosen to be released from each emission grid cell of background run

184   and in-situ run, respectively. Output data in form of $CHBr_3$ volume mixing ratios available at a user-

185   defined grid, is retrieved at a horizontal resolution of 1º x 1º and 0.5º x 0.5º for background runs and in-

Atmospheric
Chemistry
and Physics
Discussions

186   situ runs, respectively, at every 100 m from 100 m to 1 km, and every 1 km from 1 km to 20 km every 3

187   hours.

188

189   **3. Atmospheric CHBr$_3$ based on open ocean background emissions**

190

191   The atmospheric CHBr$_3$ mixing ratios diagnosed from the uniform background emissions (referred to as

192   CHBr$_3$ background mixing ratios hereinafter) vary significantly from campaign to campaign and also

193   within each campaign region. Figures 2 to 4 present several snapshots of the CHBr$_3$ background mixing

194   ratios and the simultaneous wind fields from ERA-Interim reanalysis for the three campaigns. For

195   TransBrom (Fig. 2), CHBr$_3$ accumulates south of 15º N with a maximum near the equator, where the

196   wind is weak. In the northern Pacific, which was dominated by an anticyclone centered around 165°E,

197   30°N, the background values are much lower. On the 10th of October 2009, two bands of extremely low

198   wind fields exist, one directly south of the equator and one tilting from 15°N to 5°N, which both coincide

199   with the highest CHBr$_3$ abundances. On the 20th of October, these two bands collided into one with

200   lowest winds centered around 165°E, where we again find very high values of CHBr$_3$ of up to 0.8 ppt.

201   For both case studies, highest values are found in the region of the lowest wind speeds or slightly shifted

202   towards the region of strongest wind shear. Regions of high wind speeds, such as the northern Pacific

203   anticyclone, on the other hand do not allow for accumulations and are characterized by very low CHBr$_3$.

204   For the SHIVA case (Fig. 3), the background CHBr$_3$ accumulates in a narrow region near Indonesia,

205   with corresponding wind fields smaller than 3 m/s. North of Indonesia, the strong easterly trade winds

206   generally above 10 m/s prevent the accumulation of higher background values within the region. Again,

207   the two case studies illustrate how changes of the wind patterns within a few days drive changes of the

208   background CHBr$_3$ distribution. Another particular example is the northward extension of the low

209   equatorial winds around 90°E on 16th November 2011, which leads to higher CHBr$_3$ north of the equator

210   up to 15°N.

211   For OASIS (Fig. 4), the wind speed is higher than in the other two regions and these strong

212   southeast/southwest trade winds associated with the Asian monsoon extend over most of the Indian

213   Ocean. Consistent with the stronger winds, the background values for the OASIS case are significantly

214   lower than for the other two cases, although they also show accumulations in certain regions. These

215   accumulations appear partially in regions of low wind speeds (e.g., near the equator between 70°E and

216   90°E on 17th of July) or in adjacent regions of high wind shear (e.g., north of the equator between 70°E

217   and 90°E for both case studies). For the latter case, the CHBr$_3$ accumulation also extends into the region

218   of high wind speeds, which is different from the distribution found for the TransBrom and SHIVA

219   regions. This difference occurs because the east coast of the Indian Subcontinent offshore is a region

220   with wind convergence (not shown), which tends to accumulate air masses therein.

221   Given that the accumulation of CHBr$_3$ background mixing ratios follows in most cases the wind field

222   patterns on a regional scale, we hypothesize that the same relationship holds on a global scale. The global

Atmospheric
Chemistry
and Physics
Discussions

223   distributions of atmospheric $CHBr_3$ based on background emissions and wind fields averaged over the

224   time periods of the SHIVA and OASIS cruise are presented in Fig. 5 and 6, respectively. We omit the

225   time period of the TransBrom case, since the background $CHBr_3$ distribution diagnosed for this period

226   is very similar to background found for the SHIVA period. The global $CHBr_3$ background mixing ratios

227   (Fig. 5a, and 6a) display a very heterogeneous distribution in spite of the uniform background emission

228   used for the simulations. Accumulations of $CHBr_3$ are again generally located in the regions of low wind

229   speeds. For the SHIVA period (November 2011), particularly high $CHBr_3$ background values of 0.3 to

230   0.4 ppt are found along the equator over the Maritime continent, West Pacific, Indian Ocean and at the

231   West coast of Africa, all of which are characterized by particularly low winds. In the Northern and

232   Southeast Pacific, the wind speed is generally higher, and the corresponding $CHBr_3$ values of less than

233   0.15 ppt are much lower than in the tropical region. For the OASIS period (July/August 2014), the global

234    $CHBr_3$ distribution is mostly reversed compared to the SHIVA period and high winds over the Indian

235   Ocean and Maritime continent lead to low $CHBr_3$ abundance in this region. The North Pacific on the

236   other hand, with low wind speeds is now a region of intense accumulation leading to 0.3-0.4 ppt of $CHBr_3$.

237   The tropical West Pacific is the only region that experiences relatively low winds during both seasons,

238   and constantly shows high $CHBr_3$ for the SHIVA and OASIS time periods.

239   The variations of the background $CHBr_3$ distribution can be generally explained by the seasonal

240   variations of the global wind field. The North Pacific and Northern Indian Ocean are dominated by the

241   East Asia Monsoon and the Monsoon of South Asia, respectively. The East Asia Monsoon is

242   characterized by strong northwesterly flow in boreal winter and weak southeasterly flow in boreal

243   summer due to the reverse of the thermal gradient between land and ocean (Webster, 1987; Ding and

244   Chan, 2005). Therefore, the accumulations of $CHBr_3$ in the North Pacific occurs during the boreal

245   summer months, rather than during boreal autumn/ early winter (TransBrom time period). The Monsoon

246   of South Asia, on the other hand, is characterized by weak northeasterly winds in boreal winter and

247   strong southwesterly winds in boreal summer (Webster, 1987; Webster et al., 1998). Thus background

248    $CHBr_3$ accumulation over the Northern Indian Ocean occurs mostly during boreal winter, while during

249   boreal summer (OASIS time period) a low $CHBr_3$ background can be expected. Because of the light

250   winds of the Inter Tropical Convergence Zone (ITCZ), a belt of relatively high $CHBr_3$ abundance exists

251   along the equator in the Northern Hemisphere, especially in the tropical Pacific and Atlantic. Strong

252   convection in the ITCZ enhances vertical transport of $CHBr_3$ out of the boundary layer, but overall the

253    $CHBr_3$ distribution is dominated by the horizontal wind fields and accompanying transport patterns. Due

254   to the more complex land-sea thermal difference, the seasonal variation of ITCZ in the West Pacific is

255   more significant than in the East Pacific (Waliser and Jiang, 2014). The relatively high accumulations of

256    $CHBr_3$ in the tropical East Pacific are confined to a narrow region near the equator for both seasons. As

257   for the tropical West Pacific, during boreal winter the ITCZ covers almost the whole Southeast Asia and

258   the high $CHBr_3$ abundances during SHIVA appear along the east coast of Malaysia. During boreal

259   summer, the ITCZ shifts northward and the high $CHBr_3$ abundances retreat northwestward.

Atmospheric
Chemistry
and Physics
Discussions

260   We assume constant $CHBr_3$ open ocean emissions of 100 pmol h^{-1} m^{-2} for our simulations in order to

261   isolate the impact on the atmospheric $CHBr_3$ distribution of atmospheric transport patterns versus the

262   impact of varying emission fields. In particular, variations of the wind fields will impact the ocean air-

263   sea flux, and emissions larger than 100 pmol h^{-1} m^{-2} might occur in regions of higher winds with little

264     $CHBr_3$ accumulation. Such variations can change the background $CHBr_3$ distribution and may allow for

265   increased mixing ratios in regions of strong winds. In addition to the wind speed, variations in the

266   atmospheric and, more importantly, the oceanic $CHBr_3$ concentrations can impact the emission strength

267   which can further change the complex atmospheric $CHBr_3$ distribution.

268

269   **4. Atmospheric $CHBr_3$ based on hotspot emissions**

270

271   Given the high variability of the atmospheric $CHBr_3$ background mixing ratios, resulting from

272   atmospheric transport processes (Section 3), it is of interest to analyze if and how much oceanic hotspot

273   emissions might impact this background distribution. In this section, we will use observational data to

274   discuss if oceanic hotspot emissions occur at the same time and location as peak atmospheric mixing

275   ratios or if the two quantities are rather uncorrelated. Furthermore, we will use FLEXPART simulations

276   to compare $CHBr_3$ mixing ratios that result from background emissions to the increased $CHBr_3$ mixing

277   ratios that result from localized hotspot emissions.

278

279   **4.1 Observed hotspot emission**

280

281   Oceanic $CHBr_3$ emissions, atmospheric $CHBr_3$ mixing ratios and the observed local surface wind speeds

282   are given in Fig. 7 for all three campaigns. The oceanic emissions of $CHBr_3$ vary substantially from

283   campaign to campaign with mean values of 261 pmol h^{-1} m^{-2} (TransBrom), 1228 pmol h^{-1} m^{-2} (SHIVA),

284   and 912 pmol h^{-1} m^{-2} (OASIS) with standard deviations of 600 pmol h^{-1} m^{-2} (TransBrom), 1460 pmol h^{-1}

285   m^{-2} (SHIVA) and 1159 pmol h^{-1} m^{-2} (OASIS), respectively. All three campaigns show periods with

286   background emissions around 100 pmol h^{-1} m^{-2} and periods with localized elevated and hotspot emissions.

287   For TransBrom, the first two thirds of the campaign show negative (air-to-sea) or very low background

288     $CHBr_3$ fluxes, while the last third was close to western Pacific islands and is characterized by overall

289   elevated emissions with sporadic hotspots of up to 4000 pmol h^{-1} m^{-2}. The SHIVA cruise track, on the

290   other hand, was mostly along the coastline, and low background emissions occur only for brief periods.

291   Most locations showed elevated emissions and hotspots occurred regularly. The OASIS cruise track

292   alternated between open ocean, upwelling and coastal areas, resulting in a large fluctuation between low

293   background and localized elevated emissions. Hotspot emissions during this campaign are largest,

294   reaching values of over 6000 pmol h^{-1} m^{-2}.

295   According to the flux parameterization applied here, the air-sea flux is determined mostly by the surface

296   wind speed and the ocean-atmosphere concentration gradient. Highest emissions are expected to occur

Atmospheric
Chemistry
and Physics
Discussions

297   during periods of high wind speed and large concentration gradients. The wind speed dominates the

298   fluxes for some regions, but not for entire campaigns. During the beginning of the TransBrom campaign

299   (Fig. 7a), the wind speed peaks at over 15m/sec while the corresponding $CHBr_3$ air-sea flux is low.

300   Higher wind speeds co-occur with high air-sea fluxes at the end of the campaign. For SHIVA (Fig. 7b)

301   and OASIS (Fig. 7c), the relation between wind speed and $CHBr_3$ emissions is more easily discernable.

302   All three campaigns demonstrate that high fluxes do not always lead to local high $CHBr_3$ mixing ratios

303   in the surface atmosphere. For example, several hotspots with oceanic emissions over 4000 pmol m^{-2} hr^{-}

304   ^{1} are found during OASIS, however, corresponding atmospheric mixing ratios are relatively low (~ 2

305   ppt). Vice versa, the highest atmospheric mixing ratios found during OASIS do not coincide with high

306   fluxes, except for the last part of the campaign. These discrepancies suggest that the local atmospheric

307   mixing ratios are driven by a complex interplay of source and loss processes driving the atmospheric

308   mixing ratios of short-lived compounds. A relatively clear connection between elevated oceanic

309   emissions and surface mixing ratios only occurs during the SHIVA campaign and during the last part of

310   the TransBrom campaign (Fig 7a and b).

311   As the campaign data shows a relation between emissions and atmospheric mixing ratios only for some

312   regions, the question arises how much of the atmospheric variability of short-lived compounds such as

313    $CHBr_3$ is impacted by the emission strengths. In order to quantify the relative contributions of elevated

314   emissions, comparisons between the computed mixing ratios over hotspots and the background

315   abundances in the atmosphere are required. In the subsequent section, we present such comparisons based

316   on the model results.

317

318   **4.2 Comparison of $CHBr_3$ from background and hotspot emissions**

319

320   In this section, we will compare the concentrations of $CHBr_3$ due to background and localized elevated

321   emissions as simulated by FLEXPART. First, atmospheric $CHBr_3$ during all three campaigns is

322   calculated based on the uniform background emission of 100 pmol h^{-1} m^{-2}. Second, atmospheric $CHBr_3$

323   resulting from strong localized emissions is simulated for the three case studies given by the campaigns.

324   Atmospheric $CHBr_3$ at different altitudes is simulated by FLEXPART, which is driven by the

325   meteorological data from ECMWF. The signatures of dynamical processes such as wind regimes,

326   weather phenomena (e.g., typhoons) and convection are captured by the model simulation and can be

327   detected in the $CHBr_3$ distribution (Fig. 8). For example, during the TransBrom campaign, the cruise

328   encountered several tropical storms in the western Pacific, one of which (Lupit, around October 14th,

329   2009) developed into a super typhoon within several days (Krüger and Quack, 2013). As shown in Fig.

330   8, an elevated $CHBr_3$ accumulation representing the structure of typhoon Lupit is clearly visible in the

331   background distribution of $CHBr_3$ at 500 m (Fig. 8d) altitude in the northern part of the western Pacific.

332   This structure is still clear at 5 km altitude (Fig. 8a), although with a weaker magnitude. For $CHBr_3$

333   emitted from localized elevated sources (Figures 8b, c, e, and f), such large scale structures are not

334 discernible due to the small spatial extent of the 0.5° or 1° emission cells and thus the limited amount of

335 overall released $CHBr_3$. A clear blob of higher abundances of atmospheric $CHBr_3$ can be seen in the

336 southern part of the western Pacific near Indonesia resulting from one of the hotspot emissions observed

337 during TransBrom (Fig. 1b). However, the background $CHBr_3$ in this area is also high in this low-wind

338 area, and thus the atmospheric signal of the up to 20 times stronger hotspot emissions (Fig. 7a) is

339 detectable for neither the 0.5° nor the 1° wide emission cells when compared to the background. Note

340 that the modelled atmospheric mixing ratios from both sources, hotspot and background emissions, are

341 smaller than the mixing ratios observed along the cruise track (Figure 7) suggesting stronger nearby

342 emissions not covered in our scenarios and observations. The signature of the hotspot emissions remains

343 in the boundary layer and cannot be seen at 5 km altitude.

344 Fig. 9 shows the atmospheric $CHBr_3$ mixing ratios during the SHIVA campaign. For the SHIVA case,

345 the distribution patterns of the background $CHBr_3$ abundances at 500 m altitude also show a very strong

346 spatial variability, despite the uniform emissions. Highest $CHBr_3$ background mixing ratios around 120º

347 E near the equator of up to 0.5 ppt are smaller than background values found during TransBrom of up to

348 0.8 ppt. The atmospheric signal of the localized elevated emissions is much stronger than during

349 TransBrom due to stronger emissions on the one hand and smaller background mixing ratios on the other

350 hand. First, for the 0.5° wide emission grids, two highly localized, atmospheric $CHBr_3$ peaks appear

351 close to the coast line near the equator around 105º E with a maximum value around 0.4 ppt. These

352 signals occur in a spot where the background is very low (0.2 ppt). However, at the same time they are

353 smaller than the maximum background values of up to 0.5 ppt in nearby regions (Fig. 9d). If the width

354 of the emission grids is extended to 1°, the localized $CHBr_3$ peaks mentioned above grow into two distinct

355 blobs near the equator of up to 0.8 ppt. These maxima along the first half of the cruise track are apparently

356 larger than the regional background concentrations (Fig. 9f). Elevated emissions during the second half

357 of the campaign with several hotspot events, on the other hand, do not show such clear atmospheric

358 signals right above.

359 At 5 km altitude, the overall background values are slightly lower, but the maximum mixing ratios are

360 still comparable to altitudes below due to the intense convection in the general region of the SHIVA

361 campaign (Fuhlbrügge et al., 2016). For the regions of localized elevated emissions, the convection is

362 less effective and maximum mixing ratios at 5 km are about 50% smaller compared to the values in the

363 boundary layer. Krystofiak et al. (2018) calculated the fractions of convective-contributed trace gases

364 from boundary layer to the upper troposphere using airborne measurements during the SHIVA campaign

365 and reported an even smaller fraction of boundary layer $CHBr_3$ in the upper troposphere (about 15% due

366 to convection). Thus only the signal of the 1° wide emission cells can be detected at 5 km, while assuming

367 that the emissions cover a smaller region of 0.5° width will render their impact in the free troposphere

368 negligible.

369 Due to the dominant southwest monsoon over the Northern Indian Ocean in boreal summer, the resulting

370 atmospheric abundances of the OASIS case (Fig. 10) for both scenarios, background and localized

Atmospheric
Chemistry
and Physics
Discussions

371   emissions, are much lower than for the other two campaigns. This is particularly surprising for the OASIS

372   hotspot emissions, which are in many cases larger than hotspot emissions during TransBrom or SHIVA.

373   In the open ocean, the atmospheric enhanced $CHBr_3$ mixing ratios resulting from the 0.5° (1°) wide

374   localized emission runs reach only 0.1 (0.2) ppt in a narrow belt near 60°E and are mostly smaller than

375   the background (around 0.15 ppt). An exception occurs near the coast of Madagascar, where both

376   background and hotspot emissions accumulate in the atmosphere. Maximum background values reach

377   up to 0.25 ppt and the hotspot signals peak with values of 0.3 ppt (0.5° wide emission cells) to 0.6 ppt

378   (1° wide emissions cells). These clear atmospheric signals of hotspot emissions are driven by the

379   enhanced coastal emissions near Madagascar. At 5 km altitude, atmospheric background values are very

380   low, and the hotspot contributions are close to zero.

381   In summary, the observed emissions during the three cruises were significantly higher than the

382   background of 100 pmol m^{-2} hr^{-1}. Our results show that such strong oceanic sources are not necessarily

383   detectable in the atmosphere, where transport processes can sometimes mask the impact of oceanic

384   emissions on the atmospheric $CHBr_3$ distribution.

385

386   **5. Summary and Discussion**

387

388   In this study, we simulated atmospheric $CHBr_3$ abundances that result from uniform marine background

389   emissions compared to hotspot emissions using the Lagrangian dispersion model FLEXPART.

390   The simulations demonstrate that uniform background emissions from the ocean result in a highly

391   variable atmospheric $CHBr_3$ distribution with accumulations taking place in regions of low wind speed.

392   This relation holds on regional and global scales revealing atmospheric transport processes as important

393   drivers of the distribution of short-lived trace gases with lifetimes in the range of days to weeks. The

394   relation between atmospheric background and wind patterns described here will allow us to better predict

395   the seasonal and regional characteristics of the tropospheric $CHBr_3$ distribution. Such knowledge will

396   provide valuable information for analyzing and interpreting atmospheric data from ship and aircraft

397   campaigns. For example, our results illustrate that low atmospheric $CHBr_3$ abundances cannot

398   necessarily be used to draw conclusions about the oceanic source strength below.

399   Comparisons between atmospheric $CHBr_3$ resulting from background and peak emissions suggest that

400   the impact of localized elevated emission on the atmospheric $CHBr_3$ distribution depends on their relative

401   strength, on their location and on the time of emission. The "visibility" of elevated emissions in the

402   atmospheric $CHBr_3$ distribution varies significantly between three cruises in the West Pacific and Indian

403   Ocean. In the open ocean, signals of elevated emissions can hardly be distinguished from the background

404    $CHBr_3$ distribution even for elevated sources extending over 1° wide source regions along the cruise

405   tracks. Near the coast, however, signals of elevated emissions are often strong enough to be distinguished

406   from the background. In particular, some of the hotspot emissions up to 100 times larger than the

407   background can be detected in the atmosphere. However, individual cases show that it is not necessarily

Atmospheric
Chemistry
and Physics
Discussions

408 the largest hotspot that gives a clear signal, but that the tug of war between fast advective transport and

409 local accumulation at the time of emission is also important.

410 The constant background emissions of 100 pmol m^{-2} hr^{-1} used in our study are based on a simplified

411 scenario and do not take coastal and upwelling maxima into account. Realistic oceanic emissions are

412 much more complex with large gradients in the above mentioned regions. Nevertheless, our results

413 demonstrate that atmospheric $CHBr_3$ signals, produced by localized elevated and even hotspot emissions,

414 orders of magnitudes larger than the average open ocean emissions, can be obliterated by the highly

415 variable atmospheric background. That is to say that transport variations of the atmosphere itself are

416 sufficient to produce high concentrations in certain regions and that high concentrations of VSLH in the

417 atmosphere do not always guarantee a strong local or regional source. For observational and modelling

418 studies of VSLS and other short-lived compounds, the impact of atmospheric transport patterns that are

419 identified here can be used for the interpretation of trace gas distributions and variability.

Atmospheric
Chemistry
and Physics
Discussions

Data availability

The emission data of cruise campaigns are available at Pangaea (http://www.pangaea.de). FLEXPART
output can be inquired from the authors.

Author contribution

Y. Jia, S. Tegtmeier designed the model experiments. Y. Jia carried out the FLEXPART calculations and
produced the figures. Y. Jia and S. Tegtmeier wrote the manuscript with contributions from all co-authors.

Competing interests

The authors declare that they have no conflict of interest.

Acknowledgements

Atmospheric
Chemistry
and Physics
Discussions

436 **References:**

437 Agus, E., Voutchkov, N., Sedlak, D. L.: Disinfection by-products and their potential impact on the quality
438   of water produced by desalination systems: a literature review. Desalination, 237:214–237, 2009.

439 Aschmann, J., Sinnhuber, B.-M., Atlas, E., and Schauffler, S.: Modeling the transport of very short-lived
440   substances into the tropical upper troposphere and lower stratosphere, Atmos. Chem. Phys., 9, 9237-
441   9247, 2009.

442 Baker, J. M., Sturges, W. T., Sugier, J., Sunnenberg, G., Lovett, A. A., Reeves, C. E., Nightingale, P. D.,
443   Penkett, S. A.: Emissions of CH3Br, organochlorines, and organoiodines from temperate
444   macroalgae. Chemosphere–Global Change Science 3, 93–106. doi:10.1016/S1465-9972(00)00021-
445   0, 2000.

446 Boudjellaba, D., Dron, J., Revenko, G., Démelas, C., Boudenne, J.L.: Chlorination by-product
447   concentration levels in seawater and fish of an industrialised bay (Gulf of Fos, France) exposed to
448   multiple   chlorinated   effluents,   Sci.   Total   Environ.,   541,   391–399.
449   https://doi.org/10.1016/j.scitotenv.2015.09.046, 2016.

450 Butler, J. H., King, D. B., Lobert, J. M., Montzka, S. A., Yvon-Lewis, S. A., Hall, B. D., Warwick, N.
451   J., Mondeel, D. J., Aydin, M., and Elkins, J. W.: Oceanic distributions and emissions of short-lived
452   halocarbons, Global Biogeochem. Cycles, 21, GB1023, doi:10.1029/2006GB002732, 2007.

453 Carpenter, L. J. and Liss, P. S.: On temperate sources of CHBr3 and other reactive organic bromine
454   gases, J. Geophys. Res., 105, 20 539–20 548, 2000.

455 Carpenter, L. J., Jones, C. E., Dunk, R. M., Hornsby, K. E., and Woeltjen, J.: Air-sea fluxes of biogenic
456   bromine from the tropical and North Atlantic Ocean, Atmos. Chem. Phys., 9, 1805–1816,
457   https://doi.org/10.5194/acp-9-1805-2009, 2009.

458 Carpenter, L. J., Reimann, S., Burkholder, J. B., Clerbaux, C., Hall, B. D., Hossaini, R., Laube, J. C., and
459   Yvon-Lewis, S. A.: Ozone-Depleting Substances (ODSs) and other gases of interest to the Montreal
460   Protocol, in: Scientific Assessment of Ozone Depletion: 2014. Global Ozone Research and
461   monitoring Project– Report N. 55, World Meteorological Organization, Geneva, Switzerland, 2014.

462 Carpenter, L. J., Dhomse, S., Dorf, M., Engel, A., Feng,W., Fuhlbrügge, S., Griffiths, P. T., Harris, N.
463   R. P., Hommel, R., Keber, T., Krüger, K., Lennartz, S. T., Maksyutov, S., Mantle, H., Mills, G. P.,
464   Miller, B., Montzka, S. A., Moore, F., Navarro, M. A., Oram, D. E., Pfeilsticker, K., Pyle, J. A.,
465   Quack, B., Robinson, A. D., Saikawa, E., Saiz-Lopez, A., Sala, S., Sinnhuber, B.-M., Taguchi, S.,
466   Tegtmeier, S., Lidster, R. T., Wilson, C., and Ziska, F.: A multi-model intercomparison of
467   halogenated very shortlived substances (TransCom-VSLS): linking oceanic emissions and
468   tropospheric transport for a reconciled estimate of the stratospheric source gas injection of bromine,
469   Atmos. Chem. Phys., 16, 9163–9187, https://doi.org/10.5194/acp-16-9163-2016, 2016.

470 Dee, D. P., Uppala, S. M., Simmons, A. J., Berrisford, P., Poli, P., Kobayashi, S., Andrae, U., Balmaseda,
471   M. A., Balsamo, G., Bauer, P., Bechtold, P., Beljaars, A. C. M., van de Berg, L., Bidlot, J., Bormann,
472   N., Delsol, C., Dragani, R., Fuentes, M., Geer, A. J., Haimberger, L., Healy, S. B., Hersbach, H.,
473   Hólm, E. V., Isaksen, L., Kållberg, P., Köhler, M., Matricardi, M., McNally, A. P., Monge-Sanz,
474   B. M., Morcrette, J.-J., Park, B.-K., Peubey, C., de Rosnay, P., Tavolato, C., Thépaut, J.-N. and
475   Vitart, F.: The ERA-Interim reanalysis: configuration and performance of the data assimilation
476   system, Q. J. Roy. Meteorol. Soc., 137, 553–597, 2011.

Atmospheric
Chemistry
and Physics
Discussions

477 Ding, Y. H., and Chan, J. C. L.: The East Asian summer monsoon: An overview, Meteorol. Atmos.
478   Phys.,89(1–4), 117–142, 2005.
479 Dvortsov, V. L., Geller, M. A., Solomon, S., Schauffler, S. M., Atlas, E. L., and Blake, D. R.: Rethinking
480   reactive halogen budgets in the midlatitude lower stratosphere, Geophys. Res. Lett., 26, 1699–1702,
481   https://doi.org/10.1029/1999gl900309, 1999.
482 Emanuel, K. A., and M. Živkovic-Rothman: Development and evaluation of a convection scheme for
483   use in climate models, J. Atmos. Sci., 56, 1766–1782, 1999.
484 Feng, W., Chipperfield, M. P., Dorf, M., Pfeilsticker, K., and Ricaud, P.: Mid-latitude ozone changes:
485   studies with a 3-D CTM forced by ERA-40 analyses, Atmos. Chem. Phys., 7, 2357–2369,
486   doi:10.5194/acp-7-2357-2007, 2007.
487 Fiehn, A., Quack, B., Hepach, H., Fuhlbrügge, S., Tegtmeier, S., Toohey, M., Atlas, E., and Krüger, K.:
488   Delivery of halogenated very short-lived substances from the west Indian Ocean to the stratosphere
489   during the Asian summer monsoon, Atmos. Chem. Phys., 17, 6723-6741, 10.5194/acp-17-6723-
490   2017, 2017.
491 Forster, C., Stohl, A., and Seibert, P.: Parameterization of Convective Transport in a Lagrangian Particle
492   Dispersion Model and Its Evaluation, J. Appl. Meteorol. Climatol., 46, 403–422,
493   doi:10.1175/JAM2470.1, 2007.
494 Fuhlbrügge, S., Krüger, K., Quack, B., Atlas, E., Hepach, H., and Ziska, F.: Impact of the marine
495   atmospheric boundary layer conditions on VSLS abundances in the eastern tropical and subtropical
496   North Atlantic Ocean, Atmos. Chem. Phys., 13, 6345–6357, doi:10.5194/acp-13-6345-2013, 2013.
497 Fuhlbrügge, S., Quack, B., Atlas, E., Fiehn, A., Hepach, H., and Krüger, K.: Meteorological constraints
498   on oceanic halocarbons above the Peruvian upwelling, Atmos. Chem. Phys., 16, 12205-12217,
499   https://doi.org/10.5194/acp-16-12205-2016, 2016.
500 Hepach, H., Quack, B., Ziska, F., Fuhlbrügge, S., Atlas, E., Krüger, K., Peeken, I., and Wallace, D. W.
501   R.: Drivers of diel and regional variations of halocarbon emissions from the tropical North East
502   Atlantic, Atmos. Chem. Phys., 14, 1255–1275, https://doi.org/10.5194/acp-14-1255-2014, 2014.
503 Hossaini, R., Chipperfield, M. P., Feng, W., Breider, T. J., Atlas, E., Montzka, S. A., Miller, B. R.,
504   Moore, F., and Elkins, J.: The contribution of natural and anthropogenic very short-lived species to
505   stratospheric bromine, Atmos. Chem. Phys., 12, 371-380, 10.5194/acp-12-371-2012, 2012.
506 Hossaini, R., Chipperfield, M. P., Montzka, S. A., Rap, A., Dhomse, S., and Feng, W.: Efficiency of
507   short-lived halogens at influencing climate through depletion of stratospheric ozone, Nat. Geosci.,
508   8, 186–190, doi:10.1038/ngeo2363, 2015.
509 Hossaini, R., Patra, P. K., Leeson, A. A., Krysztofiak, G., Abraham, N. L., Andrews, S. J., Archibald, A.
510   T., Aschmann, J., Atlas, E. L., Belikov, D. A., Bönisch, H., Carpenter, L. J., Dhomse, S., Dorf, M.,
511   Engel, A., Feng,W., Fuhlbrügge, S., Griffiths, P. T., Harris, N. R. P., Hommel, R., Keber, T.,
512   Krüger, K., Lennartz, S. T., Maksyutov, S., Mantle, H., Mills, G. P., Miller, B., Montzka, S. A.,
513   Moore, F., Navarro, M. A., Oram, D. E., Pfeilsticker, K., Pyle, J. A., Quack, B., Robinson, A. D.,
514   Saikawa, E., Saiz-Lopez, A., Sala, S., Sinnhuber, B.-M., Taguchi, S., Tegtmeier, S., Lidster, R. T.,
515   Wilson, C., and Ziska, F.: A multi-model intercomparison of halogenated very short-lived
516   substances (TransCom-VSLS): linking oceanic emissions and tropospheric transport for a
517   reconciled estimate of the stratospheric source gas injection of bromine, Atmos. Chem. Phys., 16,
518   9163–9187, https://doi.org/10.5194/acp-16-9163-2016, 2016.

519   Klick, S., and Abrahamsson, K.: Biogenic volatile iodated hydrocarbons in the ocean, J. Geophys. Res.,
520   97, 12,683– 12,687, 1992.

521   Krüger, K. and Quack, B.: Introduction to special issue: the Trans-Brom Sonne expedition in the tropical
522   West Pacific, Atmos. Chem. Phys., 13, 9439–9446, doi:10.5194/acp-13-9439-2013, 2013.

523   Krysztofiak, G., Catoire, V., Hamer, P. D, Marécal, V., Robert, C., Engel, A., Bönisch, H., Grossmann,
524   K., Quack, B., Atlas., E., and Pfeilsticker, K.: Evidence of convective transport in tropical West
525   Pacific   region   during   SHIVA   experiment.   Atmos.   Sci.   Lett.,   19:e798.
526   https://doi.org/10.1002/asl.798, 2018.

527   Law, K. S., Sturges, W. T., Blake, D. R., Blake, N. J., Burkeholder, J. B., Butler, J. H., Cox, R. A.,
528   Haynes, P. H., Ko, M. K.W., Kreher, K., Mari, C., Pfeilsticker, K., Plane, J. M. C., Salawitch, R. J.,
529   Schiller, C., Sinnhuber, B. M., von Glasow, R., Warwick, N. J., Wuebbles, D. J., and Yvon-Lewis,
530   S. A.: Halogenated Very Short-Lived Substances, in: Scientific Assessment of Ozone Depletion:
531   2006. Global Ozone Research and Monitoring Project–Report No. 50, World Meteorological
532   Organization, Geneva, Switzerland, 2006.

533   Lennartz, S. T., Marandino, C. A., von Hobe, M., Cortes, P., Quack, B., Simo, R., Booge, D., Pozzer,
534   A., Steinhoff, T., Arevalo-Martinez, D. L., Kloss, C., Bracher, A., Röttgers, R., Atlas, E., and
535   Krüger, K.: Direct oceanic emissions unlikely to account for the missing source of atmospheric
536   carbonyl sulfide, Atmos. Chem. Phys., 17, 385-402, https://doi.org/10.5194/acp-17-385-2017,
537   2017.

538   Liang, Q., Stolarski, R. S., Kawa, S. R., Nielsen, J. E., Douglass, A. R., Rodriguez, J. M., Blake, D. R.,
539   Atlas, E. L., and Ott, L. E.: Finding the missing stratospheric Bry: a global modeling study of CHBr3
540   and CH2Br2, Atmos. Chem. Phys., 10, 2269–2286, https://doi.org/10.5194/acp-10-2269-2010,
541   2010.

542   Liang, Q., Atlas, E., Blake, D., Dorf, M., Pfeilsticker, K., and Schauffler, S.: Convective transport of
543   very short lived bromocarbons to the stratosphere, Atmos. Chem. Phys., 14, 5781–5792,
544   https://doi.org/10.5194/acp-14-5781-2014, 2014.

545   Liu, Y., Yvon-Lewis, S., Thornton, D., Butler, J., Bianchi, T., Campbell, L., Hu, L., and Smith, R.:
546   Spatial and temporal distributions of bromoform and dibromomethane in the Atlantic Ocean and
547   their relationship with photosynthetic biomass, J. Geophys. Res.-Oceans, 118, 3950–3965, 2013.

548   Marandino, C. A., Tegtmeier, S., Krüger, K., Zindler, C., Atlas, E. L., Moore, F., and Bange, H. W.:
549   Dimethylsulphide (DMS) emissions from the western Pacific Ocean: a potential marine source for
550   stratospheric sulphur?, Atmos. Chem. Phys., 13, 8427-8437, https://doi.org/10.5194/acp-13-8427-
551   2013, 2013.

552   Montzka, S. A. and Reimann, S.: Ozone-depleting substances and related chemicals, in Scientific
553   Assessment of Ozone Depletion: 2010, Global Ozone Research and Monitoring Project–Report No.
554   52, Geneva, Switzerland, 2011.

555   Ordóñez, C., Lamarque, J. F., Tilmes, S., Kinnison, D. E., Atlas, E. L., Blake, D. R., Sousa Santos, G.,
556   Brasseur, G., and Saiz-Lopez, A.: Bromine and iodine chemistry in a global chemistry-climate
557   model: description and evaluation of very short-lived oceanic sources, Atmos. Chem. Phys., 12,
558   1423–1447, https://doi.org/10.5194/acp-12-1423-2012, 2012.

559   Palmer, C. J. and Reason, C. J.: Relationships of surface bromoform concentrations with mixed layer
560   depth and salinity in the tropical oceans, Global Biogeochem. Cy., 23, GB2014,
561   https://doi.org/10.1029/2008gb003338, 2009.
562   Quack, B. and Wallace, D. W. R.: Air-sea flux of bromoform: Controls, rates, and implications, Global
563   Biogeochem. Cy., 17, p.1023, https://doi.org/10.1029/2002gb001890, 2003.
564   Quack, B., E. Atlas, G. Petrick, V. Stroud, S. Schauffler, and D. W. R. Wallace: Oceanic bromoform
565   sources for the tropical atmosphere, Geophys. Res. Lett., 31, L23S05, doi:10.1029/2004GL020597,
566   2004.
567   Quack, B., Atlas, E., Petrick, G., and Wallace, D. W. R.: Bromoform and dibromomethane above the
568   Mauritanian upwelling: Atmospheric distributions and oceanic emissions, J. Geophys. Res., 112,
569   D09312, https://doi.org/10.1029/2006jd007614, 2007.
570   Quack, B. und Krüger, K. (Eds.): RV SONNE Fahrtbericht/Cruise Report SO218 SHIVA 15.–
571   29.11.2011 Singapore – Manila, Philippines Stratospheric Ozone: Halogens in a Varying
572   Atmosphere Part 1: SO218 – SHIVA Summary Report (in German) Part 2: SO218 – SHIVA English
573   reports of participating groups GEOMAR Report, N. Ser. 012, GEOMAR Helmholtz-Zentrum für
574   Ozeanforschung, Kiel, Germany, 112 pp., doi:10.3289/GEOMAR_REP_NS_12_2013
575   (http://oceanrep.geomar.de/22284/), 2013.
576   Randel, W. J., Park, M., Emmons, L., Kinnison, D., Bernath, P., Walker, K. A., Boone, C., and
577   Pumphrey, H.: Asian monsoon transport of pollution to the stratosphere, Science, 328, 611–613,
578   https://doi.org/10.1126/science.1182274, 2010.
579   Rex, M., Wohltmann, I., Ridder, T., Lehmann, R., Rosenlof, K., Wennberg, P., Weisenstein, D., Notholt,
580   J., Krüger, K., Mohr, V., and Tegtmeier, S.: A tropical West Pacific OH minimum and implications
581   for stratospheric composition, Atmos. Chem. Phys., 14, 4827-4841, https://doi.org/10.5194/acp-14-
582   4827-2014, 2014.
583   Salawitch, R., Weisenstein, D., Kovalenko, L., Sioris, C., Wennberg, P., Chance, K., Ko, M., and
584   McLinden, C.: Sensitivity of ozone to bromine in the lower stratosphere, Geophys. Res. Lett., 32,
585   L05811, doi:10.1029/2004GL021504, 2005.
586   Solomon, S., Garcia, R. R., and Ravishankara, A. R.: On the role of iodine in ozone depletion, J.
587   Geophys. Res.-Atmos., 99, 20491–20499, https://doi.org/10.1029/94jd02028, 1994.
588   Stemmler, I., Rothe, M., Hense, I., and Hepach, H.: Numerical modelling of methyl iodide in the eastern
589   tropical Atlantic, Biogeosciences, 10, 4211–4225, https://doi.org/10.5194/bg-10-4211-2013, 2013.
590   Stohl, A., Hittenberger, M., and Wotawa, G.: Validation of the lagrangian particle dispersion model
591   FLEXPART against largescale tracer experiment data, Atmos. Environ., 32, 4245–4264,
592   doi:10.1016/S1352-2310(98)00184-8, 1998.
593   Stohl, A. and Thomson, D. J.: A density correction for Lagrangian particle dispersion models, Boundary-
594   Lay. Meteorol., 90, 155–167, doi:10.1023/A:1001741110696, 1999.
595   Stohl, A. and Trickl, T.: A textbook example of long-range transport: Simultaneous observation of ozone
596   maxima of stratospheric and North American origin in the free troposphere over Europe, J.
597   Geophys. Res., 104, 30445, doi:10.1029/1999JD900803, 1999.
598   Stohl, A., Forster, C., Frank, A., Seibert, P., and Wotawa, G.: Technical note: The Lagrangian particle
599   dispersion model FLEXPART version 6.2, Atmos. Chem. Phys., 5, 2461–2474, doi:10.5194/acp-5-
600   2461-2005, 2005.

Atmospheric
Chemistry
and Physics
Discussions

601   Tegtmeier, S., Krüger, K., Quack, B., Atlas, E. L., Pisso, I., Stohl, A., and Yang, X.: Emission and
602   transport of bromocarbons: from the West Pacific Ocean into the stratosphere, Atmos. Chem. Phys.,
603   12, 10633-10648, 10.5194/acp-12-10633-2012, 2012.
604   Tegtmeier, S., Krüger, K., Quack, B., Atlas, E., Blake, D. R., Boenisch, H., Engel, A., Hepach, H.,
605   Hossaini, R., Navarro, M. A., Raimund, S., Sala, S., Shi, Q., and Ziska, F.: The contribution of
606   oceanic methyl iodide to stratospheric iodine, Atmos. Chem. Phys., 13, 11869-11886, 10.5194/acp-
607   13-11869-2013, 2013.
608   Tegtmeier, S., Ziska, F., Pisso, I., Quack, B., Velders, G. J. M., Yang, X., and Krüger, K.: Oceanic
609   bromoform emissions weighted by their ozone depletion potential, Atmos. Chem. Phys., 15, 13647–
610   13663, doi:10.5194/acp-15-13647-2015, 2015.
611   Warwick, N. J., Pyle, J. A., Carver, G. D., Yang, X., Savage, N. H., O'Connor, F. M., and Cox, R. A.:
612   Global modeling of biogenic bromocarbons, J. Geophys. Res.-Atmos., 111, D18311,
613   https://doi.org/10.1029/2006jd007264, 2006.
614   Waliser, D. E., and Jiang, X.: Tropical Meteorology: Intertropical Convergence Zone, Encycl., Atmos.
615   Sci., 2nd edn, Elsevier, doi:10.1016/B978-0-12-382225-3.00417-5, 2014.
616   Webster, P. J.: The Elementary Monsoon, 32 pp., John Wiley, NewYork, 1987.
617   Webster, P. J., Magaña, V. O., Palmer, T. N., Shukla, J., Tomas, R. A., Yanai, M., and Yasunari, T.:
618   Monsoons: Processes, predictability, and theprospects for prediction,J. Geophys. Res.,103(C7),
619   14,451–14,510, doi:10.1029/97JC02719, 1998.
620   Yang, J. S.: Bromoform in the effluents of a nuclear power plant: a potential tracer of coastal water
621   masses, Hydrobiologia, 464, 99–105, https://doi.org/10.1023/A:1013922731434, 2001
622   Ziska, F., Quack, B., Abrahamsson, K., Archer, S. D., Atlas, E., Bell, T., Butler, J. H., Carpenter, L. J.,
623   Jones, C. E., Harris, N. R. P., Hepach, H., Heumann, K. G., Hughes, C., Kuss, J., Krüger, K., Liss,
624   P., Moore, R. M., Orlikowska, A., Raimund, S., Reeves, C. E., Reifenhäuser, W., Robinson, A. D.,
625   Schall, C., Tanhua, T., Tegtmeier, S., Turner, S., Wang, L., Wallace, D., Williams, J., Yamamoto,
626   H., Yvon-Lewis, S., and Yokouchi, Y.: Global sea-to-air flux climatology for bromoform,
627   dibromomethane   and   methyl   iodide,   Atmos.   Chem.   Phys.,   13,   8915–8934,
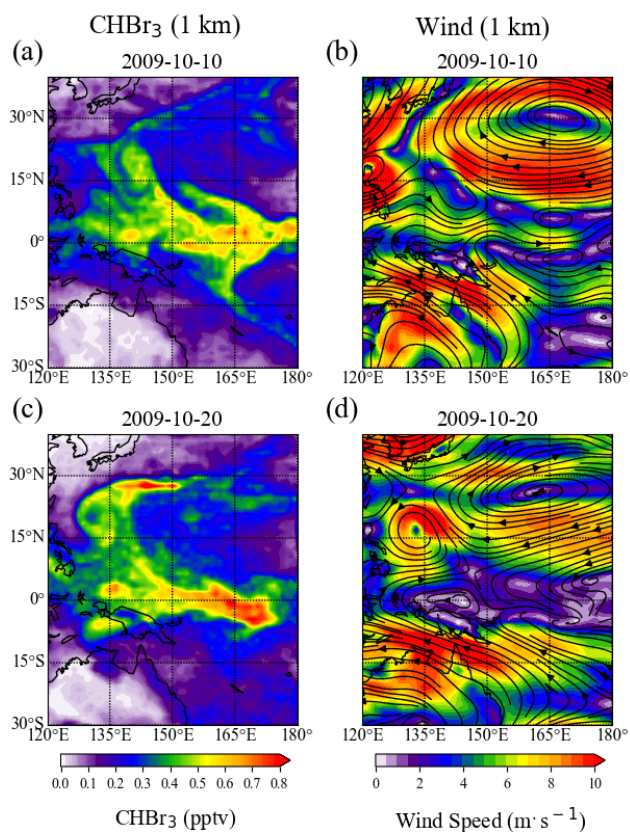628   https://doi.org/10.5194/acp-13-8915-2013, 2013.
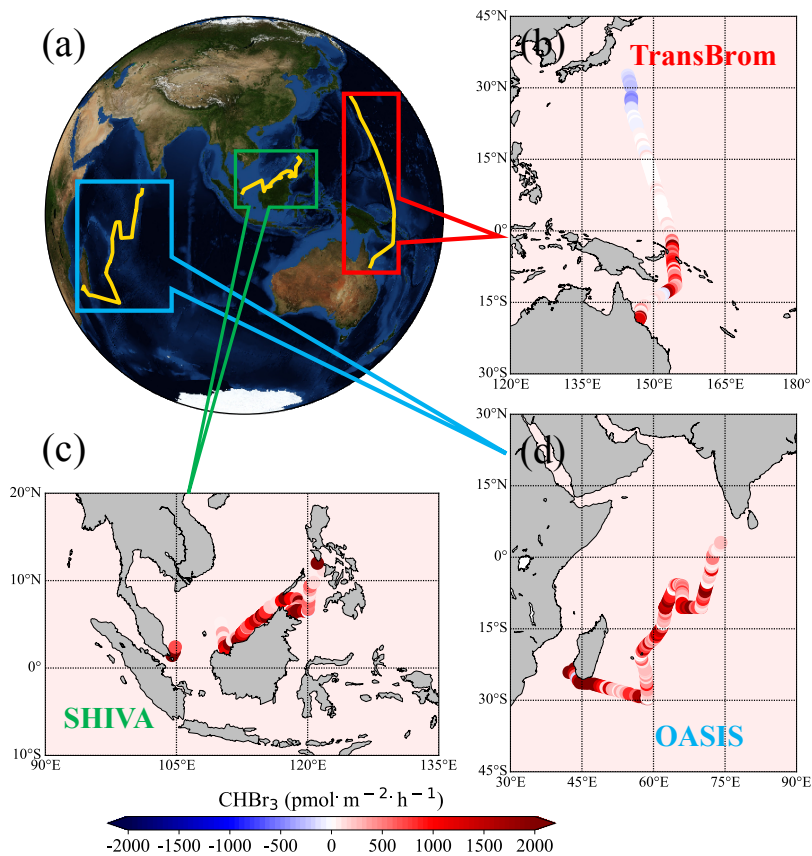
Fig 1. Cruise tracks of the three campaigns in the Indian Ocean and Western Pacific (a) and CHBr$_3$ emissions (b, c, d) used in the model simulation. Global background emissions (100 pmol m^{-2} hr^{-1}) and observed emissions along the tracks of the three research cruises TransBrom (b), SHIVA (c), and OASIS (d).
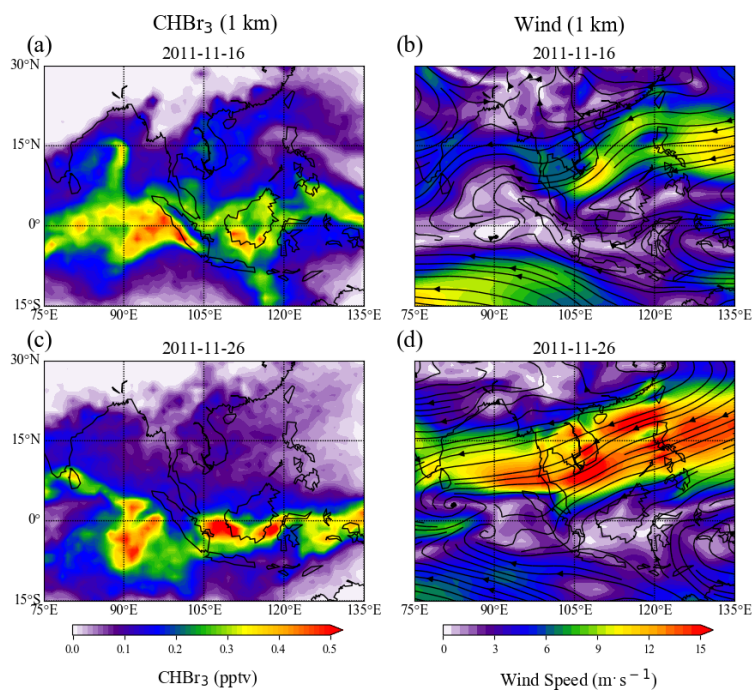
Fig. 2. Two snapshots of spatial distributions of atmospheric $CHBr_3$, derived from uniform oceanic background emissions of 100 pmol m^{-2} hr^{-1} (a, c), and ERA-Interim reanalysis wind fields (b, d) at 1 km altitude during TransBrom. The wind speed is denoted by color shades and the directions are denoted by the stream lines.

Atmospheric
Chemistry
and Physics
Discussions

Fig. 3. Same as Fig. 2, but for SHIVA case.
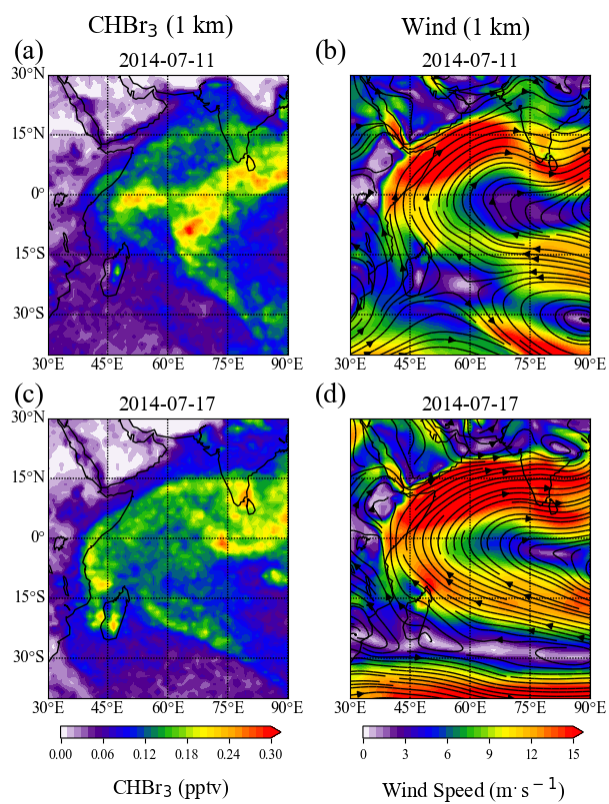
Fig. 4. Same as Fig. 2, but for OASIS case.

Atmospheric
Chemistry
and Physics
Discussions
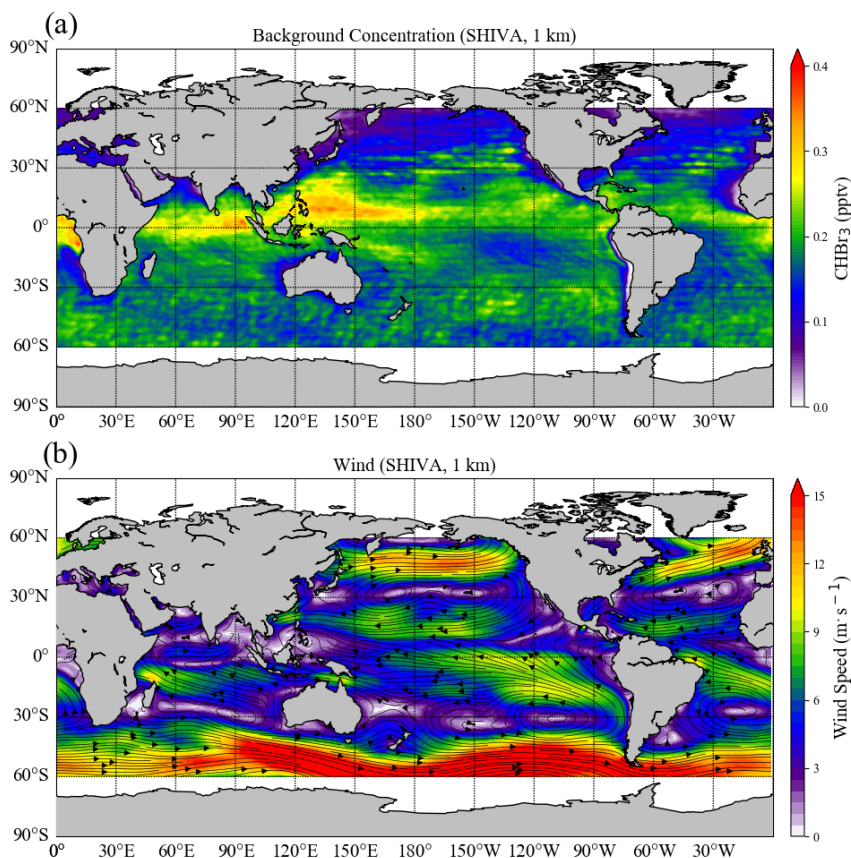
Fig. 5. Global distributions of CHBr$_3$ mixing ratios based on oceanic background emissions (a), and ERA-Interim reanalysis wind fields (b) averaged during the time period of the SHIVA cruise at 1 km. The wind speeds are denoted by color shades and the directions are denoted by the stream lines.
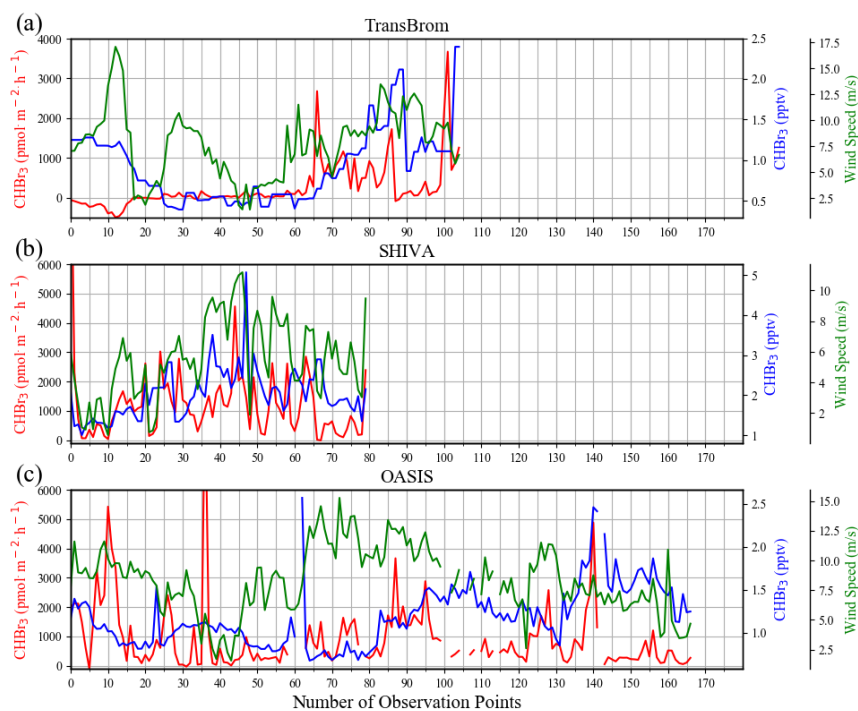
Atmospheric
Chemistry
and Physics
Discussions
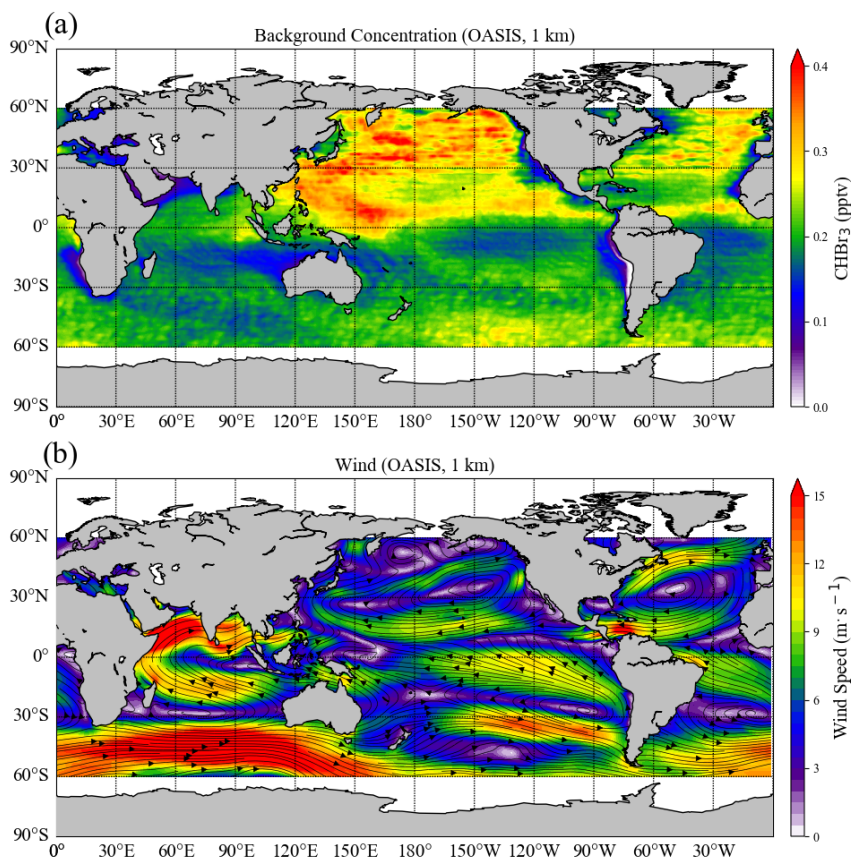
658

659   **Fig. 6.** Same as Fig. 5 but for OASIS case.

660

661

662

663

664 **Fig. 7.** Surface wind speeds (green), CHBr$_3$ air-sea flux (red), and atmospheric mixing
665 ratios of CHBr$_3$ near surface (blue) observed during TransBrom, SHIVA, and OASIS
666 campaigns.

667
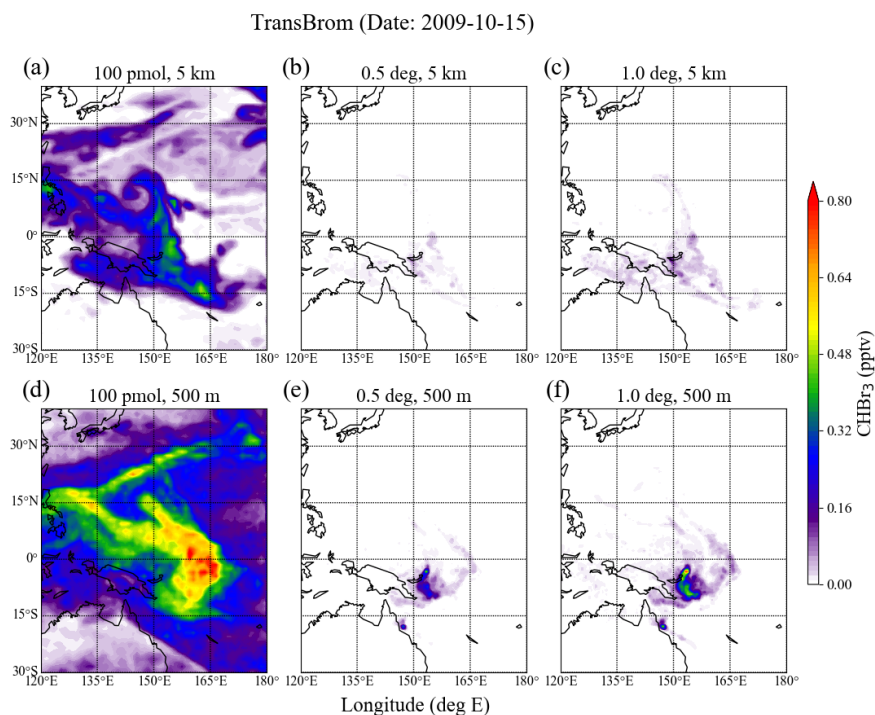
Fig. 8. Atmospheric CHBr$_3$ mixing ratios at different altitudes (500 m and 5 km) simulated for the time period of the TransBrom campaign. Simulations are based on background emissions (a, d), and elevated emissions observed during the campaign for 0.5° (b, e) and 1° (c, f) wide emission grid cells.
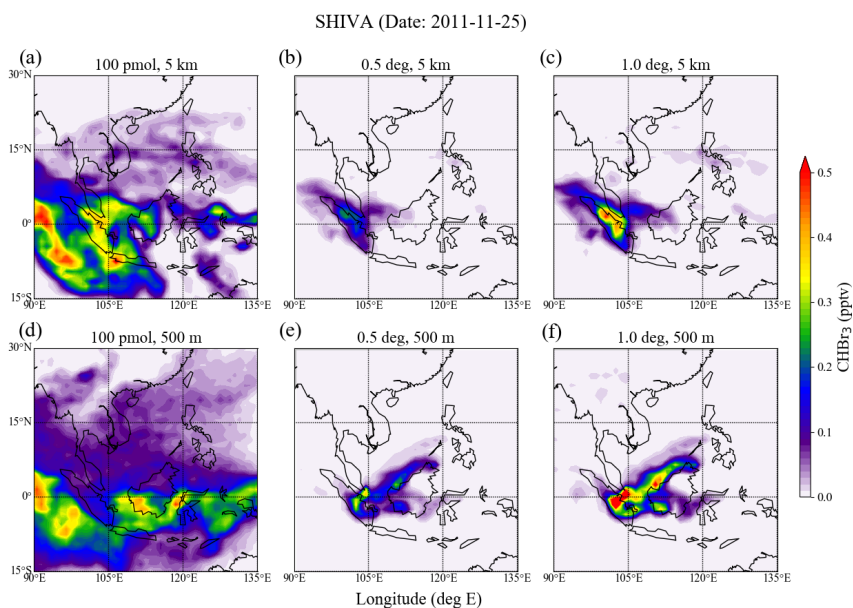
Fig. 9. Same as Fig. 8, but for the SHIVA campaign.

Atmospheric
Chemistry
and Physics
Discussions

Open Access
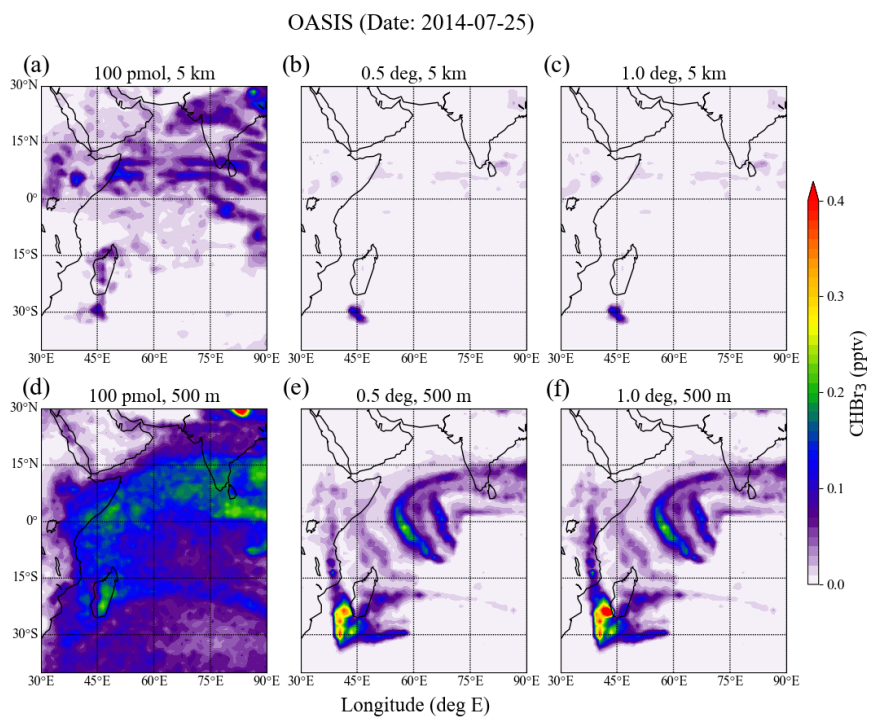
Fig. 10. Same as Fig. 8, but for the OASIS campaign.